Pannexins in ischemia-induced neurodegeneration

Panagiotis Bargiotas[a,b,c,1,2], Antje Krenz[b,2,3], Sheriar G. Hormuzdi[c,d], Dirk A. Ridder[a], Anne Herb[c,e], Waleed Barakat[b], Silvia Penuela[f], Jakob von Engelhardt[c,e], Hannah Monyer[c,e,4,5], and Markus Schwaninger[a,b,4,5]

[a]Institute of Experimental and Clinical Pharmacology and Toxicology, University of Lübeck, 23538 Lubeck, Germany; [b]Department of Pharmacology and [c]Department of Clinical Neurobiology, University of Heidelberg, 69120 Heidelberg, Germany; [e]German Cancer Research Center (DKFZ), 69120 Heidelberg, Germany; [d]Centre for Neuroscience, Ninewells Hospital and Medical School, University of Dundee, Dundee DD1 9SY, Scotland, United Kingdom; and [f]Department of Anatomy and Cell Biology, University of Western Ontario, London, ON, Canada N6A-5C1

Edited* by Michael V. L. Bennett, Albert Einstein College of Medicine, Bronx, NY, and approved November 4, 2011 (received for review December 8, 2010)

Pannexin 1 (Px1, Panx1) and pannexin 2 (Px2, Panx2) form large-pore nonselective channels in the plasma membrane of cells and were suggested to play a role in the pathophysiology of cerebral ischemia. To directly test a potential contribution of pannexins in ischemia-related mechanisms, we performed experiments in *Px1*$^{-/-}$, *Px2*$^{-/-}$, and *Px1*$^{-/-}$*Px2*$^{-/-}$ knockout mice. IL-1β release, channel function in astrocytes, and cortical spreading depolarization were not altered in *Px1*$^{-/-}$*Px2*$^{-/-}$ mice, indicating that, in contrast to previous concepts, these processes occur normally in the absence of pannexin channels. However, ischemia-induced dye release from cortical neurons was lower, indicating that channel function in *Px1*$^{-/-}$*Px2*$^{-/-}$ neurons was impaired. Furthermore, *Px1*$^{-/-}$*Px2*$^{-/-}$ mice had a better functional outcome and smaller infarcts than wild-type mice when subjected to ischemic stroke. In conclusion, our data demonstrate that Px1 and Px2 underlie channel function in neurons and contribute to ischemic brain damage.

ATP release | gap junctions | macrophage | middle cerebral artery occlusion | metabolic inhibition

Pannexins and connexins have a similar protein structure, although they seem to have evolved independently and do not share homology at the amino acid sequence level. Like connexins, pannexins may form a single membrane channel referred to as pannexon or pannexin hemichannel in the literature. Pannexons are pores in the plasma membrane allowing the passage of substances with a molecular weight of up to about 1,000 Da. Whereas opposing connexin-based hemichannels can form gap junctions between cells, channels formed by pannexins connect the cytoplasm and extracellular space (1) and appear to only form gap junctions under certain circumstances (2, 3). In mammals, three pannexins, Px1, Px2, and Px3, have been identified. Whereas Px3 is only found in the skin and Px2 is confined to the CNS, *Px1* is widely expressed (2). Heterologous expression in *Xenopus* oocytes showed that Px1 forms pannexons in the membrane (2, 4, 5). Whether Px2 on its own can form functional channels, has remained controversial (2, 6). However, coexpression of *Px2* with *Px1* generated channels with distinct properties, suggesting that Px1/Px2 heteromeric channels may form in cells coexpressing the two proteins (2, 6). In addition to ions, metabolites such as ATP can also pass through heterologously expressed pannexin channels (4).

Px1 channels have been implicated in several cellular functions. Intriguingly, many cellular effects that have been attributed to Px1 are involved in the pathophysiology of cerebral ischemia (7). To begin with, Px1 is apparently required for activating caspase 1 and releasing IL-1β from macrophages, which is of paramount importance for ischemic brain damage (8). Cleavage of pro–IL-1β to mature IL-1β by caspase 1 and the release of IL-1β are controlled by the binding of extracellular ATP to its membrane receptor $P2X_7$, which has been shown to interact with Px1, although details of the underlying molecular mechanism are still unclear (9–11). The ability of Px1 to mediate caspase-1 activation was also demonstrated in neural cells (12).

Inspired by the finding that heterologous expression of *Px1* allows for the efflux of ATP (4), recent publications provided evidence that endogenous Px1 mediates ATP release in several cell types. ATP efflux from erythrocytes through Px1 channels under hypoxic conditions may induce vasodilation (13, 14). In apoptotic lymphocytes, ATP release through Px1 channels was reported to serve as a "find-me" signal for attracting macrophages (15). Furthermore, recent evidence suggested that ATP release in astrocytes is mediated by Px1 and not by connexin 43 as previously proposed (16). Once released in the ischemic brain, ATP promotes propagation of intercellular calcium waves. Calcium waves were formerly considered to be the cellular basis of cortical spreading depolarization (CSD), a wave of depolarization that propagates slowly in the gray matter and further compromises the ischemic tissue (17). It is now clear that CSD and calcium waves are two distinct processes (18). Nevertheless, there is pharmacological evidence that the propagation of CSD relies on hemichannels or gap junctions (19–21). The molecular composition of these hemichannels, however, is not known.

In hippocampal neurons the glutamate agonist NMDA induced channel activity that showed the pharmacological and electrophysiological characteristics of pannexons (22). These channels were also activated by oxygen glucose deprivation, an in vitro model of cerebral ischemia (23). Experimentally, channel opening can be evaluated by assessing the release of preloaded dyes such as calcein green (molecular weight, 622 g/mol). Interestingly, the retention of calcein green and other dyes is also used to monitor cell vitality, giving rise to the notion that increased channel activity can promote imminent cell death (1). The opening of large, nonselective pores in the neuronal membrane is thought to contribute to anoxic depolarization, to the loss of essential metabolites such as ATP and glutathione, and to the release of toxic compounds (7), all of which promote neuronal cell death. Until now the molecular composition of these neuronal channels has remained unclear.

To investigate the involvement of Px1 and Px2 in these ischemic processes in vivo, we generated *Px2*$^{-/-}$ mice and used *Px1*$^{-/-}$ (24), the *Px2*$^{-/-}$, and *Px1*$^{-/-}$*Px2*$^{-/-}$ mice in our experiments. The mice are viable and show no obvious developmental or behavioral abnormality. Surprisingly, IL-1β production, channel activity in astrocytes, and CSD were not affected by deficiency of Px1 and

Author contributions: H.M. and M.S. designed research; P.B., A.K., S.G.H., D.A.R., A.H., W.B., and J.v.E. performed research; H.M. contributed new reagents/analytic tools; P.B., A.K., D.A.R., S.P., J.v.E., and M.S. analyzed data; and P.B., A.K., S.G.H., J.v.E., H.M., and M.S. wrote the paper.

The authors declare no conflict of interest.

*This Direct Submission article had a prearranged editor.

[1]Present address: Department of Neurology, University of Heidelberg, Im Neuenheimer Feld 400, 69120 Heidelberg, Germany.

[2]P.B. and A.K. contributed equally to this work.

[3]Present address: Department of Microbiology and Immunology, College of Veterinary Medicine, Cornell University, Ithaca, NY 14853.

[4]H.M. and M.S. contributed equally to this work.

[5]To whom correspondence may be addressed. E-mail: markus.schwaninger@pharma.uni-luebeck.de or h.monyer@Dkfz-Heidelberg.de.

This article contains supporting information online at www.pnas.org/lookup/suppl/doi:10.1073/pnas.1018262108/-/DCSupplemental.

Px2. Our studies do, however, demonstrate that channel activity in cortical neurons depends on the presence of either Px1 or Px2. This effect was relevant in vivo because $Px1^{-/-}Px2^{-/-}$ mice were significantly protected in a model of ischemic stroke.

Results

Production of Mature IL-1β in Cerebral Ischemia Does Not Depend on the Presence of Pannexins. Experiments with a peptidergic Px1 inhibitor and knockdown of *Px1* have suggested that Px1 is required for the release of IL-1β from macrophages in response to ATP (9). To reassess this concept, we compared IL-1β release from peritoneal macrophages of wild-type $Px1^{+/+}Px2^{+/+}$ and double-knockout $Px1^{-/-}Px2^{-/-}$ mice. After LPS pretreatment, ATP stimulated the release of IL-1β, as shown previously (Fig. 1*A*) (9). However, unlike as previously suggested, IL-1β release did not differ between $Px1^{+/+}Px2^{+/+}$ and $Px1^{-/-}Px2^{-/-}$ macrophages (Fig. 1*A*).

Next, we investigated IL-1β production in vivo during cerebral ischemia (8). To induce permanent focal cerebral ischemia, we occluded the middle cerebral artery (MCAO) by microbipolar electrocoagulation. Indeed, we found elevated levels of IL-1β in the ischemic hemisphere 20 h after MCAO (Fig. 1*B*). IL-1β levels measured by ELISA did not differ in wild-type $Px1^{+/+}Px2^{+/+}$, double-heterozygous $Px1^{+/-}Px2^{+/-}$, or double-knockout $Px1^{-/-}Px2^{-/-}$ mice (Fig. 1*B*). As ELISA does not distinguish reliably between mature extracellular IL-1β and intracellular pro–IL-1β, we also determined pro–IL-1β (31 kDa) levels in the same samples by Western blot. There was no difference between genotypes and hemispheres (Fig. 1*C*), implying that elevated IL-1β levels measured by ELISA in the ischemic hemispheres reflected mature IL-1β.

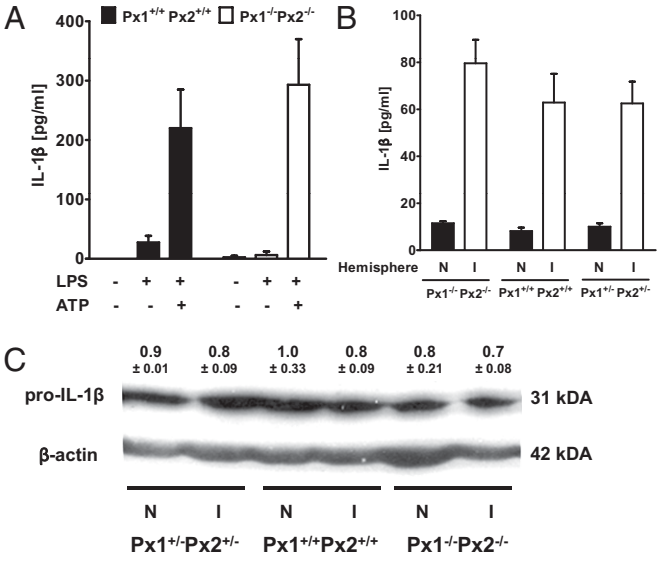

Fig. 1. IL-1β production does not depend on Px1 and Px2. (*A*) LPS- and ATP-induced release of IL-1β from macrophages did not depend on Px1 and Px2. Peritoneal macrophages from $Px1^{+/+}Px2^{+/+}$ or $Px1^{-/-}Px2^{-/-}$ mice were stimulated with LPS (100 μg/mL) for 4 h and then with ATP (5 mM) for 30 min. IL-1β was measured in the medium. Values are mean ± SEM (n = 5–9). (*B*) After middle cerebral artery occlusion, total IL-1β was higher in the ischemic (I) than in the nonischemic (N) hemispheres but did not differ significantly between wild-type $Px1^{+/+}Px2^{+/+}$, double-knockout $Px1^{-/-}Px2^{-/-}$, and double-heterozygous $Px1^{+/-}Px2^{+/-}$ mice. Total IL-1β, including pro–IL-1β and mature IL-1β, was determined in brain extracts by ELISA. Values are mean ± SEM (n = 5). (*C*) In the same samples pro–IL-1β (31 kDa) was determined by Western blot analysis. Quantification revealed no significant difference in pro–IL-1β normalized to actin between hemispheres and genotypes (two-way ANOVA). Mean values ± SEM out of two to three experiments are shown above a representative blot.

Channel Function Is Not Altered in Astrocytes of Pannexin Knockout Mice. *Px1* and *Px2* are expressed by neurons and astrocytes (Fig. 2*A*). Using an siRNA knockdown strategy, Iglesias and colleagues inferred that Px1 is a structural substrate of astrocytic channels (16). Thus, knockdown of *Px1* significantly reduced the release of ATP from astrocytes in response to 3-*O*-(4-benzoyl)benzoyl adenosine trisphosphate (BzATP), a $P2X_7$ agonist. We sought to reproduce this experiment in wild-type $Px1^{+/+}Px2^{+/+}$ and $Px1^{-/-}Px2^{-/-}$ primary astrocytes. As shown in previous studies, BzATP stimulated ATP release from astrocytes and this effect was blocked by carbenoxolone (Cbx, 100 μM), an inhibitor of pannexons and connexin hemichannels. Surprisingly, there was no difference in ATP release between $Px1^{-/-}Px2^{-/-}$ and $Px1^{+/+}Px2^{+/+}$ astrocytes (Fig. 2*B*).

To further test the role of pannexins in astrocytic channel function, we investigated the ability of astrocytes obtained from the different genotypes to release a channel-permeant dye. $Px1^{+/+}Px2^{+/+}$ or $Px1^{-/-}Px2^{-/-}$ astrocytes loaded with calcein green and treated with BzATP showed a similar decrease in fluorescence intensity, indicating a normal dye release in astrocytes devoid of Px1 and Px2 (Fig. 2*C*).

Astrocytes express channels that open in response to a voltage ramp protocol (−60 to +100 mV) (16). Currents mediated via

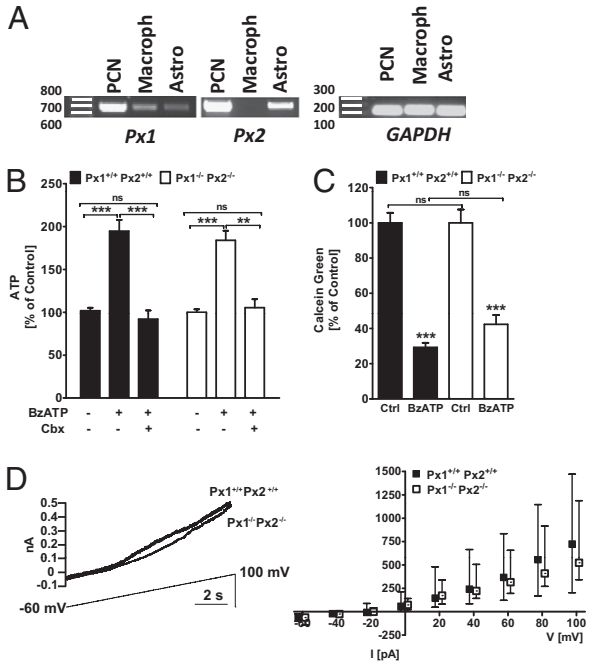

Fig. 2. Channel activity in astrocytes does not depend on Px1 and Px2. (*A*) Expression of *Px1* and *Px2* mRNA in primary cortical neurons (PCN), macrophages (macroph), and astrocytes. mRNA was detected by RT-PCR. (*B*) BzATP-induced ATP release in primary astrocytes was blocked by carbenoxolone (Cbx, 100 μM) but was not affected by the deficiency of Px1 and Px2. Bz-ATP, 300 μM. Values are mean ± SEM. Two-way ANOVA revealed a significant effect of BzATP treatment, $F(2/169) = 44.37$, $P < 0.0001$. ***$P < 0.001$ (Bonferroni post hoc test). NS, not significantly different compared with untreated control cells. (*C*) BzATP-induced calcein green dye release from astrocytes was independent of Px1 and Px2. Calcein green fluorescence intensity was measured 750 s after stimulation by BzATP and expressed as percentage of untreated controls (Ctrl). Values are mean ± SEM. Two-way ANOVA revealed a significant effect of BzATP treatment, $F(1/108) = 142.6$, $P < 0.0001$. ***$P <$ 0.001 (Bonferroni post hoc test). NS, not significantly different compared with $Px1^{+/+}Px2^{+/+}$ group. (*D*) Outward current induced by a voltage ramp (−60 to +100 mV) did not differ between astrocytes of $Px1^{+/+}Px2^{+/+}$ and $Px1^{-/-}Px2^{-/-}$ mice. (*Left*) Example recordings from single astrocytes. (*Right*) Quantification showing median values ± IQR of current amplitude at increasing voltages.

these channels were shown to be sensitive to gap junction blockers, and siRNA-mediated knockdown experiments indicated that pannexons may be the substrate of the voltage-dependent channels (16). We tested this hypothesis by performing similar voltage ramp experiments on astrocytes from wild-type $Px1^{+/+}Px2^{+/+}$ and $Px1^{-/-}Px2^{-/-}$ mice and observed no significant difference in the currents evoked for either genotype (Fig. 2*D*). These electrophysiological experiments, in addition to the previous ones examining astrocytic function in response to BzATP, demonstrate that the formation and function of astrocytic hemichannels is preserved in the absence of Px1 and Px2 and may rely on connexin 43 as shown in a previous report (25).

CSD Is Not Altered in Pannexin Knockout Mice. Previous work has suggested that hemichannels or gap junctions are involved in the propagation of CSD events (19–21). To evaluate the role of Px1 and Px2 in this process, we recorded direct current (DC) potentials and laser Doppler flow (LDF) from the cortex of anesthetized mice for 10 min before and 60 min after MCAO. CSD events were identified as DC deflections accompanied by a LDF response. This protocol has successfully demonstrated that connexin 36 is involved in CSD propagation. In $Px1^{+/+}Px2^{+/+}$ and $Px1^{-/-}Px2^{-/-}$ mice, no differences were observed in the number of CSD events in their amplitude, or duration, or in interval between events (Fig. S1 and Table S1), suggesting that the CSD propagation does not depend on pannexins.

Loss of Channel Function in Neurons from Pannexin Knockout Mice. Previous work showed that oxygen glucose deprivation of hippocampal neurons opened channels that had electrophysiological and pharmacological characteristics of pannexons (23). To test for the involvement of specific pannexin channels, we repeated those experiments on neurons obtained from pannexin knockout mice. We loaded primary cortical neurons with calcein green acetoxymethyl ester (AM) and monitored the fluorescence intensity of individual neurons for 750 s (Fig. 3*A*). Under basal conditions the fluorescence intensity remained stable, indicating that calcein green did not leak out of the cells (Fig. 3*B*). However, after metabolic inhibition by exposing cells to NaCN (2 mM), a well-known uncoupler of mitochondrial respiration, we observed a steady decrease in fluorescence that could be blocked by pretreating cells with Cbx (100 μM, Fig. 3 *B* and *D*). These findings indicate that membrane channels mediate the release of calcein green. We can exclude membrane rupture as a cause of dye leakage because lactate dehydrogenase (LDH) concentration in the medium did not increase during the 750-s observation period (Fig. S2). Dye release was slightly decreased in $Px1^{+/-}Px2^{+/-}$ neurons ($P < 0.05$) and there was a nonsignificant trend toward less dye release in $Px1^{-/-}Px2^{+/-}$ and $Px1^{+/-}Px2^{-/-}$ neurons (Fig. 3*D*). However, in double-knockout $Px1^{-/-}Px2^{-/-}$ neurons, dye release was completely blocked (Fig. 3 *C* and *D*). This confirms that Px1 and Px2 are involved in establishing neuronal channels that permit the free passage of molecules after metabolic inhibition.

Pannexin Deletion Results in Reduced Ischemic Damage. To investigate the role of pannexons in focal cerebral ischemia, we occluded the middle cerebral artery in wild-type $Px1^{+/+}Px2^{+/+}$, $Px1^{-/-}$, $Px2^{-/-}$, and double-knockout $Px1^{-/-}Px2^{-/-}$ littermate mice. Physiological parameters that are known to influence the outcome of cerebral ischemia were not altered in double-knockout mice in comparison with wild-type littermates (Table S2). Before and 24 h after MCAO, we evaluated neurological deficits using the corner test and by measuring latency to move. In the corner test, mice turn more often to the right side after left-sided MCAO (26). Wild-type, $Px1^{-/-}$, and $Px2^{-/-}$ mice exhibited right side preference after left side MCAO, but the preference did not differ among the genotypes (Fig. 4 *A* and *B*).

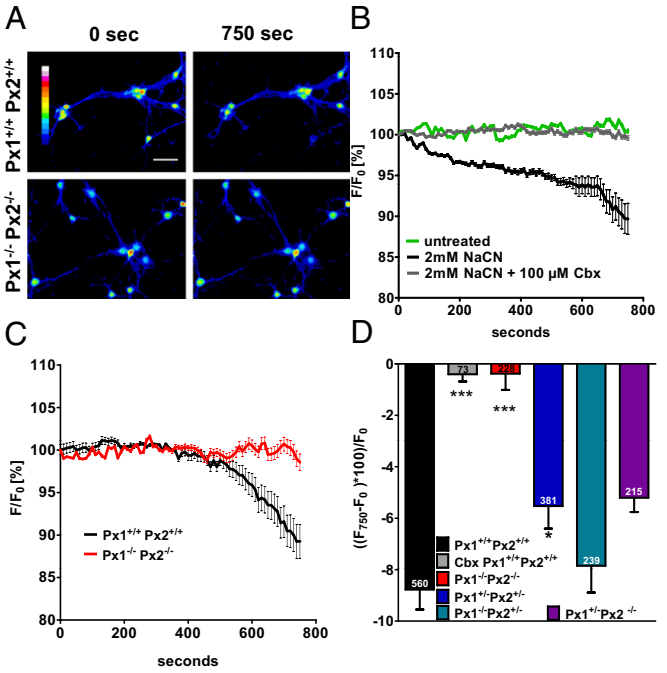

Fig. 3. In cortical neurons Px1 and Px2 are required for channel activity induced by metabolic inhibition. Calcein green-loaded primary cortical neurons were subjected to NaCN (2 mM) and fluorescence was imaged for 750 s. Decrease of fluorescence intensity indicated dye release through pannexons. (*A*) Representative image of $Px1^{+/+}Px2^{+/+}$ and $Px1^{-/-}Px2^{-/-}$ neurons before and 750 s after NaCN. Intensity is color coded. (Scale bar, 100 μm.) (*B*) Carbenoxolone (Cbx, 100 μM) inhibited dye release induced by NaCN from wild-type neurons. The time course of fluorescence intensity expressed as a percentage of the starting value (F_0) in a single experiment is shown. (*C*) Dye release in response to NaCN was inhibited in $Px1^{-/-}Px2^{-/-}$ neurons. Values of a single experiment with 91 $Px1^{+/+}Px2^{+/+}$ and 52 $Px1^{-/-}Px2^{-/-}$ cells are shown. (*D*) Mean values of the fluorescence change (F_{750}–F_0) × 100/F_0 in five to seven independent experiments 750 s after applying NaCN. The total number of cells evaluated per condition is given in the bars. One-way ANOVA, $F(5/1,690) = 12.66$, $P < 0.0001$; $^*P < 0.05$, $^{***}P < 0.001$ in comparison with $Px1^{+/+}Px2^{+/+}$ cells (Bonferroni post hoc test).

In contrast, in double-knockout mice the right side preference was significantly lower than in wild-type animals after MCAO, reflecting an improvement in neurological deficit (Fig. 4*C*). As expected, the latency to move was increased after MCAO in wild-type mice. $Px1^{-/-}$ knockout mice showed a trend to reduced latencies after MCAO (Fig. 4*D*). However, in $Px2^{-/-}$ single and $Px1^{-/-}Px2^{-/-}$ double-knockout mice, the latencies were significantly shorter than in wild-type mice after MCAO (Fig. 4*F*). In keeping with these observations, the infarct volume was not significantly reduced in $Px1^{-/-}$ single-knockout mice 48 h after MCAO (Fig. 4*G*). Although $Px2^{-/-}$ single-knockout mice were partially protected in functional assays, they did not show a significant reduction of the infarct size (Fig. 4*H*). However, the infarct size was 40% lower in $Px1^{-/-}Px2^{-/-}$ double-knockout mice (Fig. 4*I*). In summary, these results demonstrate that Px1 and Px2 channels contribute to ischemic brain damage in vivo.

Discussion

Several important cellular functions have been ascribed to Px1 channels. To reassess the role of pannexins and to investigate their functions in vivo, we generated *Px1* and *Px2* knockout mice. The animals are viable and fertile, and no morphological changes were observed in the brain by histological analysis. Our experiments suggest that pannexins are not required for the ATP-induced release of IL-1β from macrophages or for hemichannel

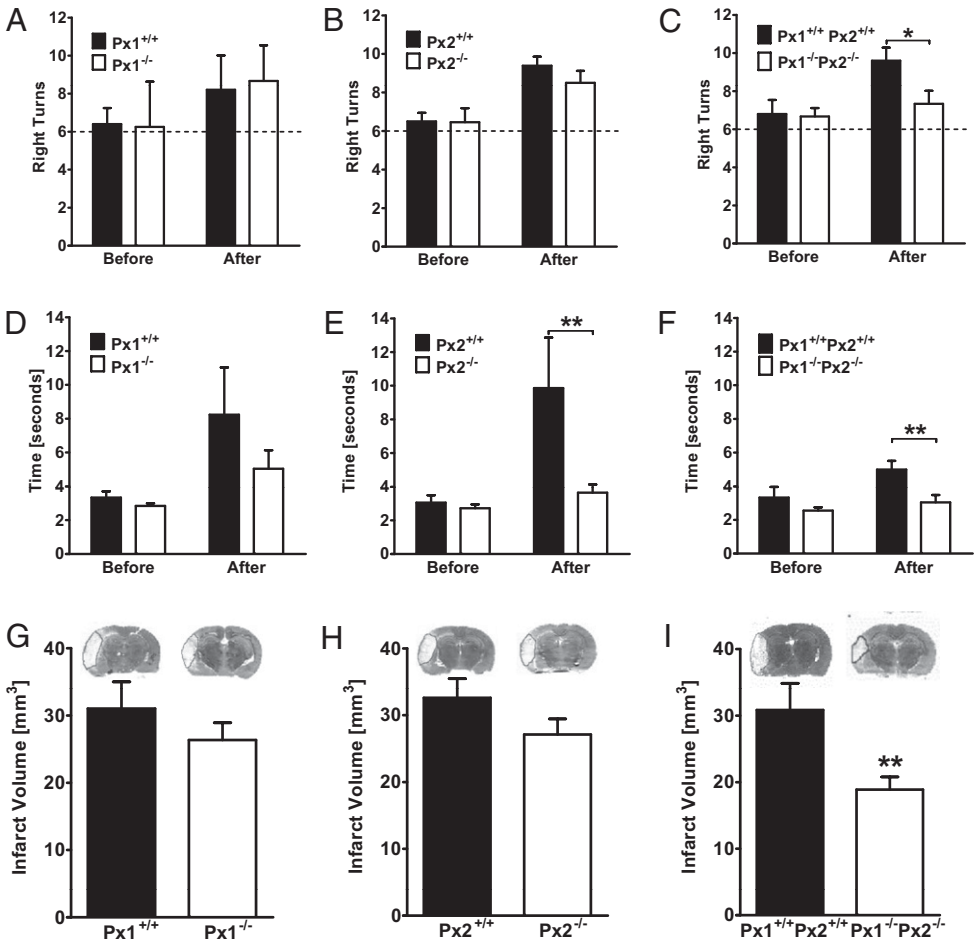

Fig. 4. Double-knockout $Px1^{-/-}Px2^{-/-}$ mice were protected in a stroke model. (*A*, *B*, *D*, and *E*) Compared with $Px1^{+/+}Px2^{+/+}$ littermates, neurological deficits did not differ in $Px1^{-/-}$ and $Px2^{-/-}$ mice after MCAO as evaluated by the corner test (*A* and *B*). When measuring latency to move, $Px1^{-/-}$ mice showed a trend (*D*) and $Px2^{-/-}$ a significantly shorter latency than wild-type littermates (*E*), $F(1/58) = 9.7$, $P < 0.01$. $^{**}P < 0.01$ (repeated-measures ANOVA). The dashed line indicates the expected behavior without a side preference in 12 trials of the corner test. Mice were investigated before and 24 h after MCAO. Values are mean ± SEM ($n = 6$–14). (*G* and *H*) $Px1^{-/-}$ and $Px2^{-/-}$ mice showed no statistically significant differences in infarct volume compared with $Px1^{+/+}Px2^{+/+}$ littermates. Values are mean ± SEM ($n = 15$–18). (*C* and *F*) Double-knockout $Px1^{-/-}Px2^{-/-}$ mice had a smaller neurological deficit 24 h after MCAO than $Px1^{+/+}Px2^{+/+}$. In the corner test (*C*), the pathological preference of $Px1^{+/+}Px2^{+/+}$ littermates to turn to the right side was significantly reduced in $Px1^{-/-}Px2^{-/-}$ mice 24 h after MCAO. $F(1/12) = 6.7$, $P < 0.05$. $^{*}P < 0.05$ (repeated-measures ANOVA, $n = 5$–9). In the latency to move (*F*), $Px1^{-/-}Px2^{-/-}$ mice needed significantly less time to move compared with their $Px1^{+/+}Px2^{+/+}$ littermates. $F(1/12) = 5.9$, $P < 0.01$. $^{**}P < 0.01$ (repeated-measures ANOVA, $n = 5$–9). (*I*) Double deletion of both *Px1* and *Px2* ($Px1^{-/-}Px2^{-/-}$) significantly reduced the infarct volume compared with the $Px1^{+/+}Px2^{+/+}$ littermates. $^{**}P < 0.01$ (*t* test, $n = 6$–10).

function in astrocytes. Previous studies leading to contrary conclusions relied on pharmacological tools or on siRNA-mediated knockdown of *Px1* (9, 10, 16). The specificity of hemichannel inhibitors such as Cbx is notoriously low (7) and even the alleged pannexin inhibitor ^{10}panx1 inhibits not only pannexins but also connexin 46 (27). In addition, many knockdown studies were based on a single siRNA corresponding to the *Px1* sequence, and rescue experiments were not performed (9, 10, 16). Thus, in these studies, unexpected off-target effects affecting the innate immune system and cytokine release cannot be excluded (28). Our data demonstrate that release of IL-1β and hemichannel function in astrocytes are not affected in the absence of Px1 and Px2. We cannot exclude at present that *Px1* and *Px2* deletion is compensated by up-regulation of other genes.

Unlike in astrocytes, in neurons, channel activity induced by metabolic inhibition depended on the presence of both Px1 and Px2, confirming a previous report (23). Whereas deletion of either *Px1* or *Px2* did not significantly affect channel activity, double knockout of *Px1* and *Px2* abrogated channel activity completely. Opening of a large, nonselective pore by energy shortage poses a considerable risk to neurons. To investigate the functional significance of channel opening in a relevant in vivo model, we subjected pannexin-deficient mice to MCAO, a model of ischemic stroke. In keeping with our findings in cultured neurons, we found that consistent protection was provided only when both Px1 and Px2 were lacking—single-knockouts of either *Px1* or *Px2* did not differ in ischemic brain damage from wild type, although $Px2^{-/-}$ mice were partially protected at the functional level. Furthermore, our finding that calcein green-loaded cortical neurons from $Px1^{-/-}Px2^{+/-}$ animals exhibit wild-type levels of dye release suggests that Px2 can form functional channels even in the absence of Px1. This is in apparent conflict with the initial characterization of pannexins showing that heterologous expression of *Px2* in *Xenopus* oocytes did not produce functional channels (2). The reason for this discrepancy is not clear at present, but one possible explanation is that, as a result of posttranslational modifications or via dimerization with other partners, Px2 can form channels in mammalian cells in the absence of Px1. Indeed, dye uptake was reported in Px2-expressing 293T cells (6). Thus, Px1 and Px2 may compensate for each other.

How might neuronal pannexons be activated in cerebral ischemia? There are several possibilities: Due to K^+ efflux the extracellular K^+ concentration increases in cerebral ischemia. This increase in extracellular K^+ concentration may be sufficient to activate neuronal Px1 channels (12). Additionally, reactive oxygen species and NO, which are abundant in ischemic brain tissue and have been shown to open pannexons in neurons, may be involved (29). The redox sensitivity of Px1 may stem from an interaction with the K^+ channel subunit Kvβ3 (30). A more protracted activation of pannexin channels may occur during apoptosis through the cleavage of Px1 by caspase 3 (15). The cleaved subunit forms constitutively open channels. It is questionable whether this mechanism is involved in the rapid opening of pannexons observed in vitro, but it may be important in vivo as caspase 3 is activated in cerebral ischemia (31). In addition to the opening of pannexin channels, cerebral ischemia may also aggravate the outcome owing to increased expression of *Px1* and *Px2* (29).

In $Px1^{-/-}Px2^{-/-}$ mice, infarcts were smaller and the neurological deficit not as great. Thus, Px1/Px2 channels are an attractive target for stroke therapy. Indeed, channel inhibitors such as Cbx were shown to be protective in stroke models (32, 33). Because Cbx and other compounds have only a low selectivity for pannexin channels over connexin gap junctions and hemichannels, it is likely that they also inhibit the protective effects of connexin 43 and connexin 32 (34, 35). Thus, our data suggest that selective pannexin inhibitors may be more efficacious in stroke treatment.

Materials and Methods

Targeting of *Px1* and *Px2*. The generation of $Px1^{-/-}$ mice has been described previously (24). Further details are presented in Fig. S3 *A* and *B*. To target the *Px2* gene, a genomic *Px2* fragment containing exon 1 was obtained after screening a 129/SvJ mouse genomic library. This fragment was modified such that a BssHII restriction endonuclease segment flanking the coding portion of *Px2* in exon 1 was replaced with a nuclear localized β-galactosidase reporter (*nLacZ*), and a loxP-flanked phosphoglycerate kinase-neomycin cassette (*PGK-neo*) was inserted into an ApaI restriction endonuclease site 3′ to the exon (Fig. S3*D*). The targeting construct was linearized and electroporated into R1 embryonic stem cells. Positive clones containing a *Px2* disrupted neo-containing allele were identified by Southern blot analysis. Two clones were injected into blastocysts and germline transmission of the mutant allele was determined by Southern blot analysis using genomic DNA obtained from chimeric mice (Fig. S3*E*). The *Px2* knockout allele used in all of these experiments was generated after removing the neomycin cassette by breeding with Cre-deleter mice. In situ hybridization on brain sections verified the successful knockout of the *Px1* and *Px2* gene (Fig. S4). *Px1* and *Px2* mRNA measured by real-time RT-PCR was not detectable in the respective knockout mice (Fig. S5), confirming that gene targeting was effective. Finally, Western blots using anti-Px1 (6) and anti-Px2 (provided by R. Dermietzel and G. Zoidl, Ruhr University, Bochum, Germany) antibodies further evidenced the successful deletion of the two pannexin genes (Fig. S6).

Genotyping for $Px1^{-/-}$ and $Px2^{-/-}$ mice was performed by standard PCR on genomic DNA extracted from mouse tail tips. The following primer pairs were used for genotyping $Px1^{-/-}$ mice: 5′-GGA AAG TCA ACA GAG GTA CCC-3′ and 5′-CTT GGC CAC GGA GTA TGT GTT-3′ (330 bp, wild-type allele), 5′-GGA AAG TCA ACA GAG GTA CCC-3′ and 5′-GTC CCT CTC ACC ACT TTT CTT ACC-3′ (630 bp, mutant allele) and for genotyping $Px2^{-/-}$ mice: 5′-TCC TGC TAT GAA GCT GGC ATC TCT G-3′ and 5′-CAA GAA GCC ACC CTT GAC TGG CAA A-3′ (350 bp, wild-type allele; 430 bp, mutant allele). See Table S3 for primers listed for RT-PCR.

Breeding of $Px1^{-/-}$ and $Px2^{-/-}$ heterozygous mice yielded homozygous knockouts at the expected Mendelian ratio. Knockout mice had been backcrossed on a C57BL/6 background for at least four generations. For all experiments we used 11- to 14-wk-old, sex-matched mice.

Middle Cerebral Artery Occlusion. The mice were subjected to left MCAO as previously described (36). Briefly, the mice were anesthetized by intraperitoneal injection of 25 μL 1.5% tribromoethanol per gram of body weight. The middle cerebral artery was exposed and occluded by microbipolar electrocoagulation (ICC 50; Erbe). The rectal temperature was maintained at 37.0 °C during surgery using a heating pad. Forty-eight hours after the permanent occlusion, the mice were reanesthetized with tribromoethanol, perfused intracardially with Ringer solution, and then the brains were carefully removed. Coronal cryosections of the brains (20 μm in thickness) were cut every 400 μm and stained with a silver technique. The size of the ischemic lesion was corrected for brain edema and determined using Scion Image software (Scion). The investigator was unaware of the genotype of mice. All animal experiments were approved by the local animal welfare committee (Regierungspräsidium Karlsruhe; Ministerium für Landwirtschaft, Umwelt und ländliche Räume, Kiel, Germany).

Release of Calcein Green and ATP. Both the ATP and the calcein green release assays were conducted in Ca^{2+}/Mg^{2+}-free PBS because it had been shown that decreased divalent cation concentrations increase the sensitivity of the ATP receptor $P2\times_7$ to its ligands ATP and BzATP (37). Confluent astrocyte cultures from $Px1^{+/+}Px2^{+/+}$ and $Px1^{-/-}Px2^{-/-}$ mice were seeded in 24-well plates, washed twice in PBS, and then treated for 3 min with BzATP (300 μM), as indicated. After complete removal and washout of the agonist, cells were bathed in PBS for 2 min before the supernatant was collected to measure ATP release (16). Cbx (100 μM) was applied 30 min before, during, and after the BzATP stimulus. ATP in the samples was analyzed using CellTiterGlo kit (Promega). Luminescence was measured on a Luminoskan Ascent plate reader (ThermoFisher) and values are expressed as percentage of untreated controls.

Confluent astrocyte cultures of $Px1^{+/+}Px2^{+/+}$ and $Px1^{-/-}Px2^{-/-}$ mice were loaded with 20 μM calcein green AM (AnaSpec) 15 min in advance, washed twice in PBS, and then stimulated with BzATP (300 μM), as indicated. Cellular calcein green fluorescence of whole wells was determined in a Fluoroskan Ascent plate reader (ThermoFisher, excitation: 485 nm, emmision: 520 nm) at the time of stimulation ($t = 0$ s) and after an additional incubation period ($t = 750$ s). Fluorescence at $t = 0$ served as internal control to normalize $t = 750$ values for cell density differences. Values were calculated as percentage of untreated control.

Primary cortical neurons (day in vitro, DIV 10–12) cultured in μ-Slide $I^{0.8}$ Luer, Ibidi, chamber slides in a volume of 300 μL were washed with 37 °C prewarmed HBSS and loaded with 20 μM calcein green AM in HBSS (PAA). After incubation for 15 min at 37 °C, cells were washed with two volumes HBBS, followed by a wash with three volumes of artificial cerebrospinal fluid (aCSF, in mM: 120 NaCl, 26 $NaHCO_3$, 3 KCl, 10 glucose, 2 $CaCl_2$, 1 $MgCl_2$). To induce metabolic inhibition, aCSF was exchanged with aCSF containing 2 mM sodium cyanide (NaCN) with or without 100 μM Cbx. Untreated controls were not exposed to NaCN. Time-lapse imaging was performed with a Nikon multiepifluorescence setup on a Nikon Eclipse Ti inverted microscope (Nikon Plan Fluor 10× NA 0.3 objective) equipped with an environmental chamber (Tokai-Hit INU chamber, Pecon CO_2 controller, set to 37 °C, 5% CO_2). Images were acquired using a Hamamatsu ORCA-AG camera every 10 s. Neurons were monitored for 10 min before applying NaCN to ensure that the calcein fluorescence signal was stable.

Electrophysiology in Vitro. To record from astrocytes patch pipettes had a resistance of 3–5 MΩ when filled with the following solution (in mM): 120 Cs-gluconate, 10 CsCl, 8 NaCl, 10 Hepes, 10 phosphocreatine-Na, 0.3 Na_3GTP, 2 MgATP, and 0.2 EGTA (pH 7.3, adjusted with NaOH). Cells were continuously superfused with buffer (22–24 °C) containing (in mM): 125 NaCl, 2.5 KCl, 2 $CaCl_2$, 1 $MgCl_2$, 1.25 NaH_2PO_4, 25 $NaHCO_3$, and 25 glucose, pH 7.2 (maintained by continuous bubbling with carbogen). A 10-s ramp protocol was applied in voltage clamp mode with depolarization of the cell from a holding potential of −60 mV to +100 mV. Currents induced by the ramp protocol were measured at different potentials (−60, −40, −20, 0, +20, +40, +60, +80, and +100 mV). Solitary astrocytes were visually identified using an upright microscope equipped with infrared-differential interference contrast. Stimulus delivery and data acquisition were performed using Pulse software (Heka Elektronik). Signals were filtered at 3 kHz, sampled at 10 kHz, and analyzed off-line with IGOR Pro (Wavemetrics).

Statistical Analysis. Data are expressed as means ± SEM with the exception of the voltage ramp experiment (Fig. 2*C*), in which median ± interquartile range (IQR) are given because data were not normally distributed. Student's *t* test was used to compare two groups. For the comparison of three or more groups one-way or two-way ANOVA followed by Bonferroni post hoc test was performed. The time course of dye release and sensorimotor function was analyzed by repeated-measures ANOVA. Values of $P < 0.05$ were considered to be significant.

For a description of other methods (recording of cortical spreading depolarization, sensorimotor testing, measurement of physiological parameters and IL-1β levels, cell culture, and RT-PCR) please refer to *SI Materials and Methods*.

ACKNOWLEDGMENTS. We thank the Nikon Imaging Center at the University of Heidelberg; Drs. R. Dermietzel and G. Zoidl for kindly providing antipannexin 2 antibodies; and Beate Lembrich for expert technical assistance. The research leading to these results received funding from the European Union's Seventh Framework Program FP7/2007–2013) under Grant agreements 201024 and 202213 (European Stroke Network).

1. MacVicar BA, Thompson RJ (2010) Non-junction functions of pannexin-1 channels. *Trends Neurosci* 33:93–102.
2. Bruzzone R, Hormuzdi SG, Barbe MT, Herb A, Monyer H (2003) Pannexins, a family of gap junction proteins expressed in brain. *Proc Natl Acad Sci USA* 100:13644–13649.
3. Lai CP, et al. (2007) Tumor-suppressive effects of pannexin 1 in C6 glioma cells. *Cancer Res* 67:1545–1554.
4. Bao L, Locovei S, Dahl G (2004) Pannexin membrane channels are mechanosensitive conduits for ATP. *FEBS Lett* 572:65–68.
5. Barbe MT, Monyer H, Bruzzone R (2006) Cell-cell communication beyond connexins: The pannexin channels. *Physiology (Bethesda)* 21:103–114.
6. Penuela S, Bhalla R, Nag K, Laird DW (2009) Glycosylation regulates pannexin intermixing and cellular localization. *Mol Biol Cell* 20:4313–4323.
7. Bargiotas P, Monyer H, Schwaninger M (2009) Hemichannels in cerebral ischemia. *Curr Mol Med* 9:186–194.
8. Allan SM, Tyrrell PJ, Rothwell NJ (2005) Interleukin-1 and neuronal injury. *Nat Rev Immunol* 5:629–640.
9. Pelegrin P, Surprenant A (2006) Pannexin-1 mediates large pore formation and interleukin-1beta release by the ATP-gated P2X7 receptor. *EMBO J* 25:5071–5082.
10. Pelegrin P, Surprenant A (2007) Pannexin-1 couples to maitotoxin- and nigericin-induced interleukin-1beta release through a dye uptake-independent pathway. *J Biol Chem* 282:2386–2394.
11. Pelegrin P, Barroso-Gutierrez C, Surprenant A (2008) P2X7 receptor differentially couples to distinct release pathways for IL-1beta in mouse macrophage. *J Immunol* 180:7147–7157.
12. Silverman WR, et al. (2009) The pannexin 1 channel activates the inflammasome in neurons and astrocytes. *J Biol Chem* 284:18143–18151.
13. Locovei S, Bao L, Dahl G (2006) Pannexin 1 in erythrocytes: Function without a gap. *Proc Natl Acad Sci USA* 103:7655–7659.
14. Sridharan M, et al. (2010) Pannexin 1 is the conduit for low oxygen tension-induced ATP release from human erythrocytes. *Am J Physiol Heart Circ Physiol* 299: H1146–H1152.
15. Chekeni FB, et al. (2010) Pannexin 1 channels mediate 'find-me' signal release and membrane permeability during apoptosis. *Nature* 467:863–867.
16. Iglesias R, Dahl G, Qiu F, Spray DC, Scemes E (2009) Pannexin 1: The molecular substrate of astrocyte "hemichannels". *J Neurosci* 29:7092–7097.
17. Somjen GG (2001) Mechanisms of spreading depression and hypoxic spreading depression-like depolarization. *Physiol Rev* 81:1065–1096.
18. Peters O, Schipke CG, Hashimoto Y, Kettenmann H (2003) Different mechanisms promote astrocyte Ca2+ waves and spreading depression in the mouse neocortex. *J Neurosci* 23:9888–9896.
19. Nedergaard M, Cooper AJ, Goldman SA (1995) Gap junctions are required for the propagation of spreading depression. *J Neurobiol* 28:433–444.
20. Margineanu DG, Klitgaard H (2006) The connexin 36 blockers quinine, quinidine and mefloquine inhibit cortical spreading depression in a rat neocortical slice model in-vitro. *Brain Res Bull* 71:23–28.
21. Largo C, Tombaugh GC, Aitken PG, Herreras O, Somjen GG (1997) Heptanol but not fluoroacetate prevents the propagation of spreading depression in rat hippocampal slices. *J Neurophysiol* 77:9–16.
22. Thompson RJ, et al. (2008) Activation of pannexin-1 hemichannels augments aberrant bursting in the hippocampus. *Science* 322:1555–1559.
23. Thompson RJ, Zhou N, MacVicar BA (2006) Ischemia opens neuronal gap junction hemichannels. *Science* 312:924–927.
24. Anselmi F, et al. (2008) ATP release through connexin hemichannels and gap junction transfer of second messengers propagate Ca2+ signals across the inner ear. *Proc Natl Acad Sci USA* 105:18770–18775.
25. Contreras JE, et al. (2002) Metabolic inhibition induces opening of unapposed connexin 43 gap junction hemichannels and reduces gap junctional communication in cortical astrocytes in culture. *Proc Natl Acad Sci USA* 99:495–500.
26. Lubjuhn J, et al. (2009) Functional testing in a mouse stroke model induced by occlusion of the distal middle cerebral artery. *J Neurosci Methods* 184:95–103.
27. Wang J, Ma M, Locovei S, Keane RW, Dahl G (2007) Modulation of membrane channel currents by gap junction protein mimetic peptides: Size matters. *Am J Physiol Cell Physiol* 293:C1112–C1119.
28. Jackson AL, Linsley PS (2010) Recognizing and avoiding siRNA off-target effects for target identification and therapeutic application. *Nat Rev Drug Discov* 9:57–67.
29. Zhang L, et al. (2008) Role for nitric oxide in permeability of hippocampal neuronal hemichannels during oxygen glucose deprivation. *J Neurosci Res* 86:2281–2291.
30. Bunse S, et al. (2009) The potassium channel subunit Kvbeta3 interacts with pannexin 1 and attenuates its sensitivity to changes in redox potentials. *FEBS J* 276:6258–6270.
31. Le DA, et al. (2002) Caspase activation and neuroprotection in caspase-3- deficient mice after in vivo cerebral ischemia and in vitro oxygen glucose deprivation. *Proc Natl Acad Sci USA* 99:15188–15193.
32. Takeuchi H, et al. (2008) Blockade of microglial glutamate release protects against ischemic brain injury. *Exp Neurol* 214:144–146.
33. de Pina-Benabou MH, et al. (2005) Blockade of gap junctions in vivo provides neuroprotection after perinatal global ischemia. *Stroke* 36:2232–2237.
34. Oguro K, et al. (2001) Global ischemia-induced increases in the gap junctional proteins connexin 32 (Cx32) and Cx36 in hippocampus and enhanced vulnerability of Cx32 knock-out mice. *J Neurosci* 21:7534–7542.
35. Nakase T, Fushiki S, Naus CC (2003) Astrocytic gap junctions composed of connexin 43 reduce apoptotic neuronal damage in cerebral ischemia. *Stroke* 34:1987–1993.
36. Murikinati S, et al. (2010) Activation of cannabinoid 2 receptors protects against cerebral ischemia by inhibiting neutrophil recruitment. *FASEB J* 24:788–798.
37. Suadicani SO, Brosnan CF, Scemes E (2006) P2X7 receptors mediate ATP release and amplification of astrocytic intercellular Ca2+ signaling. *J Neurosci* 26:1378–1385.